Available online at www.sciencedirect.com
SCIENCE DIRECT
Thermochimica Acta 430 (2005) 115–122
thermochimica acta
www.elsevier.com/locate/tca

Analysis of the sensitivity and sample–furnace thermal-lag of a differential thermal analyzer

P. Roura, J. Farjas *

GRMT, Department of Physics, University of Girona, Campus Montilivi, Edif. PII E17071 Girona, Catalonia, Spain

Received 6 September 2004; received in revised form 7 January 2005; accepted 10 January 2005
Available online 8 February 2005

Abstract

The heat exchange between the horizontal furnace of a differential thermal analyzer (DTA) and the sample is analyzed with the aim of understanding the parameters governing the thermal signal. The resistance due to radiation and conduction through the gas has been calculated and compared to the experimental values of the thermal-lag between the sample and furnace and apparatus sensitivity. The overall evolution of these parameters with the temperature and their relative values are well understood by considering the temperature differences that arise between the sample and holder. Two RC thermal models are used for describing the apparatus performance at different temperature ranges. Finally, the possibility of improving the signal quality through the control of the leak resistances is stressed.
© 2005 Elsevier B.V. All rights reserved.

Keywords: Differential thermal analysis; Thermal-lag; Sensitivity

1. Introduction

Differential scanning calorimetric techniques are used to analyze the heat that evolves during structural transformations (both physical and chemical) of materials. The experiments are quicker, simpler and require a smaller amount of sample than with traditional calorimetric techniques such as adiabatic calorimetry. This is usually achieved at the expense of temperature resolution and enthalpy accuracy [1]. To evaluate the sample temperature, calibration procedures are well established. Most of them are based on the well-known relationship [2]:

$$T_S = T_F - \tau\beta + \Delta T_C$$

where T_S and T_F are the sample and furnace temperatures, respectively, β is the heating rate (dT/dt) and ΔT_c is an offset independent of β. The time constant τ depends on the sample heat capacity, C_S, and two characteristic parameters of the apparatus, R_0 and τ_x:

$$\tau = \tau_x + R_0 C_S$$

where R_0 is a thermal resistance. Usually, the effect of the apparatus on the signal shape and intensity is modeled by simple thermal models involving a set of 'thermal masses' (C_i) and resistances (R_i) that result in characteristic time-constants [2–4].

The performance of a differential calorimeter depends on these parameters which determine its sensitivity and its ability to resolve different peaks. A number of works are devoted to the analysis, from this point of view, of the quality of the thermal signal [5,6]. An even greater number of papers analyze the deviations from the ideal peak shape by considering the contact resistances between sample and pan or pan and holder [7,8], or the temperature gradients that develop into the sample [9,10]. This last effect is especially important in temperature modulated differential scanning calorimetry (TMDSC) [9] and it was one key subject to the classical differential thermal analysis (DTA) [11] technique. The val-

* Corresponding author. Tel.: +34 972 41 83 83; fax: +34 972 41 80 98.
E-mail addresses: pere.roura@udg.es (P. Roura), jordi.farjas@udg.es (J. Farjas).

0040-6031/$ – see front matter © 2005 Elsevier B.V. All rights reserved.
doi:10.1016/j.tca.2005.01.020

ues of time-constants, thermal resistances and heat capacities are obtained from calibration procedures [2,12]. In contrast, these thermal parameters are seldom predicted from an analysis of the temperature distribution within the measuring cell of the calorimeter, as a result, calculations leading to these values are scarce.

After doing an extensive revision of the literature, we have found very few papers, if any, that predict the thermal parameters of any differential scanning calorimeter (DSC or DTA). From our point of view, the degree of knowledge at this level is quite poor and is reduced to the general concepts of heat transport. In fact, for most practitioners of thermal analysis, this level of comprehension is enough (for instance, in Ref. [3], the elementary models of DSC apparatus that are described in Section 2 are proposed without any detailed analysis of heat transport). However, if one is interested in improving the signal of a differential calorimeter, it is essential to understand the physical paths for heat transport. A review of the attempts done in this direction can be found in a recent paper by Ozawa [13] where the work of Boersma [14] is qualified as crucial in the development of differential calorimetry. After his analysis of the heat transfer mechanisms in a 'classical DTA', Boersma concluded that quantitative measurements by this technique were inherently impossible. Several papers followed which tried to improve the performance of DTA. As shown in the paper by Wilburn et al. [15], one solution consists in introducing an external resistance between the sample and furnace in such a way that the thermal gradients into the sample become negligible in most experiments. Although these gradients are minimized in most modern DSC apparatus, they are relevant in modulated DSC [16,17]. All these papers deal with heat transport indeed; on the other hand, we found no one that deduced the thermal parameters of any particular DSC or DTA apparatus. Additionally, no one treated the problem of heat exchange by radiation (the main transport mechanism of our DTA).

In this paper we present a study devoted to understanding the experimental values of the thermal parameters of a DTA equipment where the heat transport from the furnace to the sample is mainly governed by thermal radiation with a smaller contribution of conduction through the gas. Fig. 1 makes clear that the thermal exchanges in our DTA are quite different from those in the 'classical' DTA technique [11,5].

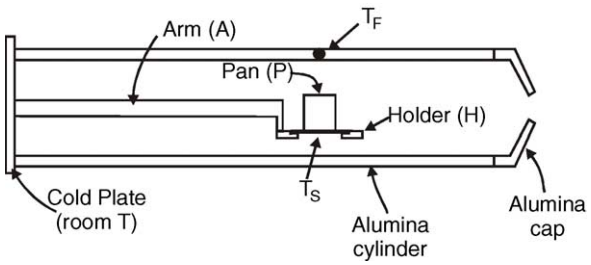

Fig. 1. Diagram of the horizontal furnace of the DTA apparatus.

In particular, in classical DTA, the thermocouples are inserted into the sample and reference materials [18]. Consequently, the thermal gradients in the sample are of crucial importance to understand the apparatus performance. In contrast, the thermal parameters of our DTA can be predicted with reasonable accuracy by considering that sample and pan have a homogeneous temperature.

The scheme in Fig. 1 is shared by a number of commercial DTA and TG/DTA (DTA simultaneous with thermogravimetry) equipment. We hope that the analysis that follows can be of help to optimize their thermal parameters through improved design.

2. Theory

2.1. Furnace and holder description

A diagram of the furnace is drawn in Fig. 1. The chamber is an alumina tube with an inner diameter of $D_F = 2.3$ cm. One side of it has good thermal contact with a cold plate, whereas the other side has an alumina cap. For the sake of simplicity, we will consider that the wall temperature is homogeneous and is measured by the 'furnace thermocouple', which is located in the alumina tube near the position of the sample. This temperature will be called the 'furnace temperature', T_F.

The sample is introduced inside an alumina pan (mass, $m_{pan} = 0.26$ g, diameter, $D_{pan} = 6$ mm and height, $h_{pan} = 5$ mm) hold by a thin platinum disc (thickness, $h_{Pt} = 0.05$ mm and diameter, $D_{Pt} = 9$ mm). A thermocouple on the back of the disc measures the so-called 'sample temperature', T_S. The thermal resistance between sample and thermocouple is not taken into account.

The platinum disc is clamped at the center of a hollow alumina disc, that we call the 'sample–holder' (external diameter, $D_{holder} = 13.5$ mm and mass, $m_{holder} = 0.4$ g). It is thinnest near the pan position with the aim of providing thermal resistance. The sample–holder is finally sustained near the axis of the furnace by a long alumina arm through which the electrical connections to the sample thermocouple are secured (diameter, $D_{arm} = 2.4$ mm and section, $A_{arm} = 3.7$ mm^2).

From the thermal point of view, this particular DTA apparatus can be modeled by the scheme drawn in Fig. 2a (Model A). The system is divided into three parts (sample and pan, sample–holder and arm) with heat capacities C_P and C_H. Thermal resistances, R_i, model the interactions between them and with the furnace. Apart from the thermal contact through the sample–holder, any interaction between the pan and arm are not considered since the thermal conductance due to the gas and radiation is much smaller than the solid path offered by the holder. In spite of its apparent simplicity, this 'complete' model is too complicated and analytical relationships are very cumbersome. In the following sections, useful simplifications are shown that can be considered for the analysis of the experimental results.

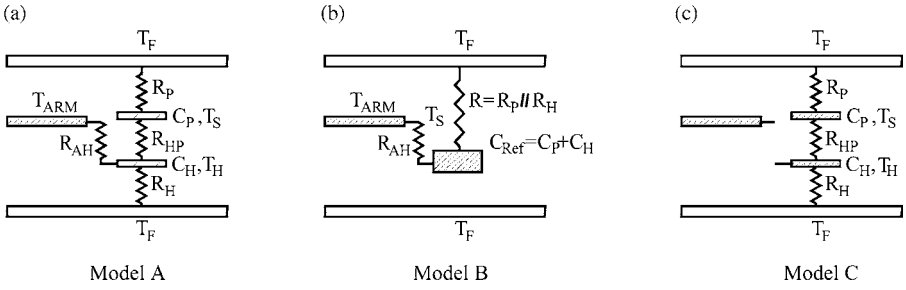

Fig. 2. (a) Thermal model that takes into account the interactions between the pan and holder and the arm and holder; (b) simplified model where the pan and sample–holder exchange heat with the furnace as a whole ($R_{HP} \ll R_P$) (Model B); (b) Model C where the thermal contact between the holder and arm is neglected ($R_{AH} \gg R_H$).

2.2. Thermal-lag between the furnace and sample–holder

During an experiment at a constant heating rate ($dT_F/dt = \beta$), the 'sample temperature' deviates from the 'furnace temperature' due to the heat that flows from the furnace, heating the sample, pan and holder (Fig. 3). It can be shown that, under very general assumptions and in the absence of any chemical reaction:

$$T_F - T_S = \tau_{LAG}\beta \tag{1}$$

where the time-constant τ_{LAG} will depend on the actual thermal conditions of the furnace. A first approximation of the τ_{LAG} value could be obtained by considering the ideal situation where thermal contact between the sample–holder and pan are perfect ($R_{HP} = 0$) and no heat is lost through the arm ($R_{AH} = \infty$). Additionally, and for the rest of the article, the sample heat capacity will not be considered. These assumptions lead to the simple thermal Model B with $R_{AH} = \infty$ in Fig. 2b and to an explicit value of τ_{LAG}:

$$\tau_{LAG}(\text{Model B}, R_{AH} = \infty) = RC_{REF} \equiv \tau_{R0} \tag{2}$$

where C_{REF} is the heat capacity of the pan and holder ($C_{REF} = C_P + C_H$) and R is the thermal resistance between them and the furnace ($R = R_P//R_H$). In fact, the thermal contact with the arm will result in a heat flow that will modify the τ_{LAG} value. It can be shown (see Appendix A) that τ_{LAG} is higher than τ_{R0} when the arm temperature is lower than T_S:

$$\tau_{LAG}(\text{Model B}) = \tau_{R0} + \frac{T_S - T_{ARM}}{\beta}\frac{R}{R_{AH}} \tag{3}$$

where R_{AH} is the thermal resistance connecting the arm to the sample–holder. This result can be interpreted as if an additional heat capacity was added to the holder. The contrary stands when the arm temperature is higher.

A useful alternative model (Model C in Fig. 2c) is that considering a finite thermal resistance, R_{HP}, between sample–holder and pan, and ignoring thermal losses to the arm. Within this model a simple analysis (see Appendix A) leads to:

$$\tau_{LAG}(\text{Model C}) = \frac{R_H + R_{HP}}{R_P + R_{HP} + R_H}R_PC_P + \frac{R_P}{R_P + R_{HP} + R_H}R_HC_H \equiv \tau_{R1} \tag{4}$$

that reduces to:

$$\tau_{LAG}(\text{Model C}, R_{HP} = \infty) = R_PC_P \equiv \tau_{R2} \tag{5}$$

Eq. (4) tells us that, within this model (Model C), τ_{LAG} is some kind of average between the thermal lag that the pan (R_PC_P) and the holder (R_HC_H) would have if they did not interact through R_{HP}. On the other hand, another interesting conclusion is that τ_{R1} approaches τ_{R0} of Eq. (2) when R_HC_H approaches R_PC_P. This conclusion is independent from the value of R_{HP}.

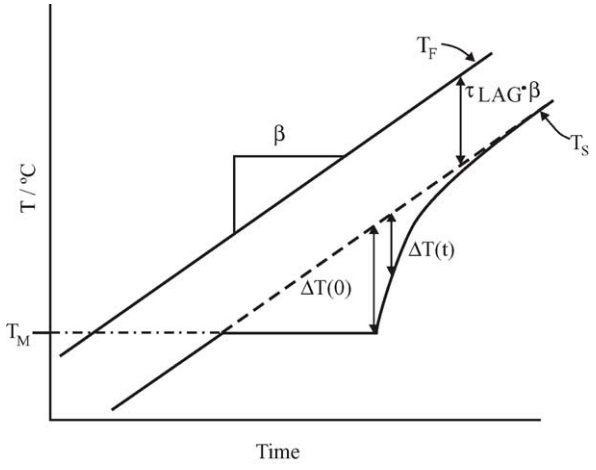

Fig. 3. Time evolution of the furnace and sample temperature when a melting process takes place at $T_S = T_M$.

2.3. Sensitivity

When the sample undergoes a structural reaction, then heat evolves and the sample temperature departs from the furnace temperature by two contributions:

$$T_F - T_S = \tau_{LAG}\beta - S\phi \tag{6}$$

where S is the sensitivity of the apparatus and ϕ is the power flowing from the pan to the furnace ($\phi > 0$ for an exothermic

reaction). The definition given here of S, is related to the signal due to a structural transformation, $\Delta T \equiv -S\phi$ (Fig. 3).

In contrast with the value of τ_{LAG}, the sensitivity is much more dependent on the thermal contact between the sample–holder and the pan. Several situations should be considered:

(1) Within Model B ($R_{HP} \ll R_P$), before any substantial amount of heat is transported to the furnace, the holder and pan will have reached a homogeneous temperature. So, heat will leave the holder and pan as a whole through the thermal resistance R and $S = R$. If thermal losses to the arm are significant, then the sensitivity will be reduced:

$$S(\text{Model B}) \leq R \tag{7}$$

(2) Within Model C, when R_{HP} increases, the evolved heat in the sample will increase the pan temperature over the sample–holder temperature. At the limit, the pan will exchange heat directly to the furnace and S will reach a maximum value equal to R_P. So:

$$S(\text{Model C}) \leq R_P \tag{8}$$

3. Experimental results

A number of experiments have been carried out in order to measure the values of τ_{LAG} and S for the entire range of furnace temperatures (from room temperature to 1500 °C). Several pure metals (In, Zn, Al, Ag, Cu and Ni) have been melted at different heating rates in argon in order to avoid oxidation. Within the range of sample masses used, the results are independent from them. This means that the heat capacity of the samples as well as the thermal gradients that could develop inside them can be ignored.

The values of τ_{LAG} have been obtained (according to Eq. (1)) from the shift of the furnace temperature at the onset of the melting process. At this point the sample begins to melt and, consequently, $T_S = T_M$. In Fig. 4 the results obtained for

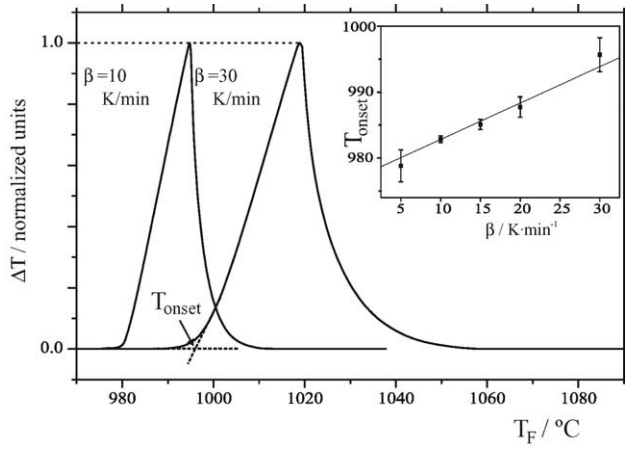

Fig. 4. Typical thermograms obtained with silver at different heating rates. In the inset, the method for extracting the value of τ_{LAG} is shown.

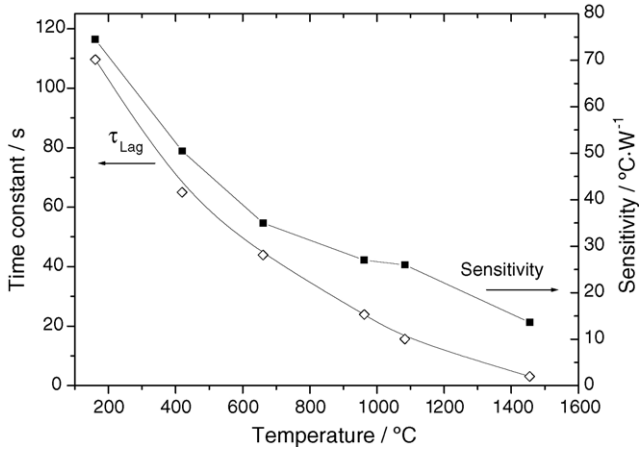

Fig. 5. Experimental values of the thermal-lag between T_S and T_F (τ_{LAG}) and the sensitivity (S).

silver (T_M(Ag) = 962 °C) are shown. In Fig. 5, τ_{LAG} is plotted versus temperature. It diminishes monotonically from 110 s at 160.6 °C to 3.1 s at 1455 °C.

Finally, the sensitivity is obtained from the area under the peak:

$$S = \frac{\int_{peak} \Delta T \, dt}{\Delta H_M} \tag{9}$$

where ΔH_M is the melting enthalpy. S diminishes monotonically as temperature increases (Fig. 5). However, it must be noted that compared to τ_{LAG} the relative variation of S is the smallest and a clear deviation from the general monotonous trend is observed around 1000 °C.

4. Analysis

In this section we will try to understand the experimental values of τ_{LAG} and S. They are analyzed in view of the theory outlined in Section 2, mainly with the help of the thermal models in Fig. 2. In addition, for quantitative analysis the thermal properties of the materials involved are needed. These values (Fig. 6) have been obtained from a number of sources:

- κ_{Pt}, c_{Pt} and $\rho_{Pt} = 21.4\ \text{g/cm}^3$ are, respectively, the thermal conductivity, specific heat capacity and mass density of platinum [19];
- κ_{AlO}, c_{AlO} and $\rho_{AlO} = 3.98\ \text{g/cm}^3$ are the values for alumina [20];
- e is the total hemispherical emissivity of alumina [21], and
- κ_{Ar} is the thermal conductivity of argon [19].

4.1. Prediction of the thermal-lag between the furnace and sample (τ_{LAG})

The heat exchange between the inner surface of the alumina tube (furnace) and the pan and sample–holder is made

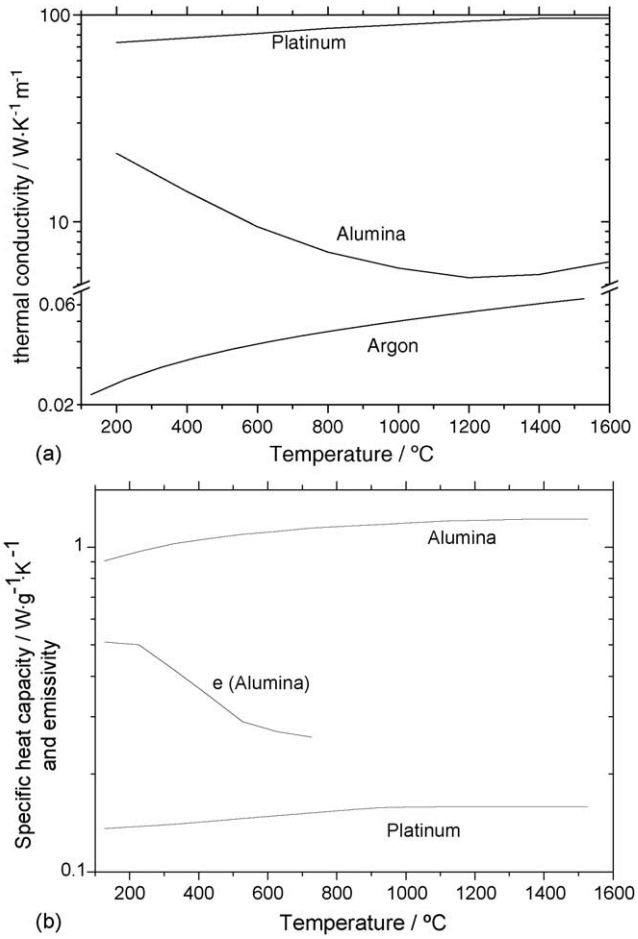

Fig. 6. Thermal properties of the materials used in the analysis.

through two transport mechanisms: conduction through the gas and radiation. The thermal resistance of each mechanism cannot be calculated exactly because of the complicated geometry of the pan and holder. So, we will consider a simplified geometrical model with an analytical solution that will keep the main functional dependencies on surface areas and thermal constants. We assume that the exact values will be proportional to the analytical ones (R_{g0} and R_{r0}) by a constant (α_g and α_r, respectively) related to the geometry and independent of temperature. Then, τ_{LAG} is calculated according to Eq. (2):

$$\tau_{LAG} = RC_{REF} = \frac{\alpha_g R_{g0} \alpha_r R_{r0}}{\alpha_g R_{g0} + \alpha_r R_{r0}} (C_P + C_H) \quad (10)$$

The thermal resistance of the reference due to radiation, R_{r0}, has been calculated by assuming that radiation is isotropic and equal to the blackbody equilibrium radiation at the furnace temperature. Any portion of the exposed surface area of pan and holder, A, are supposed to absorb the same amount of radiation. So, shadowing effects are neglected. Under these assumptions:

$$R_{r0} = \frac{1}{4A\sigma_B e T^3} \quad (11)$$

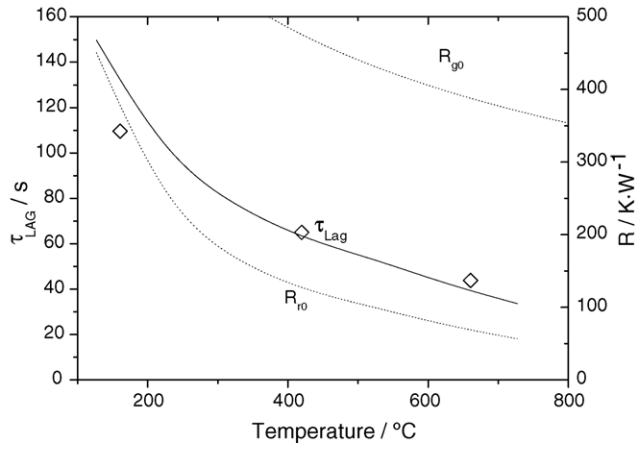

Fig. 7. Comparison between the experimental and calculated values of τ_{LAG}. The thermal resistances due to heat transport through the gas and due to radiation are also shown.

where σ_B is the Stephan–Boltzmann constant. The result is plotted in Fig. 7 for the range of temperatures where the experimental value of e is available [21].

For calculating the resistance due to the gas, the pan and sample–holder are modeled by a cylinder of length $L_g = 14$ mm (equal to the diameter of the sample–holder) and diameter $D_g = 0.70$ cm, such that the lateral surface equals the exposed surface area of the pan and holder. If cylindrical symmetry is assumed, then:

$$R_{g0} = \frac{1}{2\pi\kappa_{Ar} L_g} \ln \frac{D_F}{D_g} \quad (12)$$

The result is also plotted in Fig. 7. This calculation assumes that the temperature distribution in the gas reaches the steady value with a time-constant, τ_g, much shorter than τ_{LAG}. This point is confirmed by the small values of τ_g obtained in a previous work ($\tau_g = 0.4$ s at 700 °C) [22]. Now τ_{LAG} can be calculated for a series of values of the free parameters α_g and α_r. However it is not necessary. In Fig. 7 it is shown that $\alpha_g = \alpha_r = 1$ corresponds reasonably well with the experimental results. This means that R_{r0} and R_{g0} can be taken as a good approximation to the real values of the thermal resistances.

At any temperature, $R_{r0} < R_{g0}$ thus indicating that radiation is the main transport mechanism. At high temperatures this conclusion is reinforced in view of the T^{-3} dependence (Eq. (11)), although this tendency is compensated somewhat by the decrease in emissivity with temperature (Fig. 6b).

In spite of the agreement between calculated and measured values of τ_{LAG}, one may ask whether the experimental value really corresponds to the pan and sample–holder as a whole (Model B with $R_{AH} = \infty$) as assumed in the calculation or if the thermal contact with the arm has a substantial influence. The answer is that, “no mater the way you calculate τ_{LAG}, the result is similar”. The thermal lag of the arm is smaller than the value of Fig. 7 by about 20%, whereas, considering the pan as isolated from the holder, its thermal lag would be about 15% higher than that of the pan and holder.

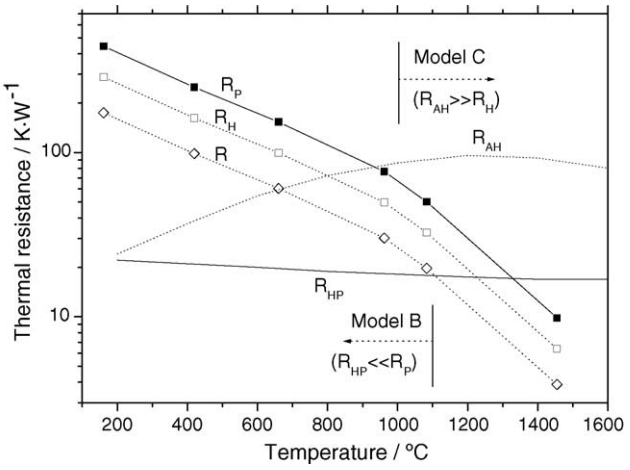

Fig. 8. Approximate values of the resistances between the pan–holder and furnace (R), the pan and furnace (R_P) and the holder and furnace (R_H) compared to the 'leak resistances' to the arm (R_{AH}) and from the pan to holder ($R_{HP} \approx R_{Pt}$).

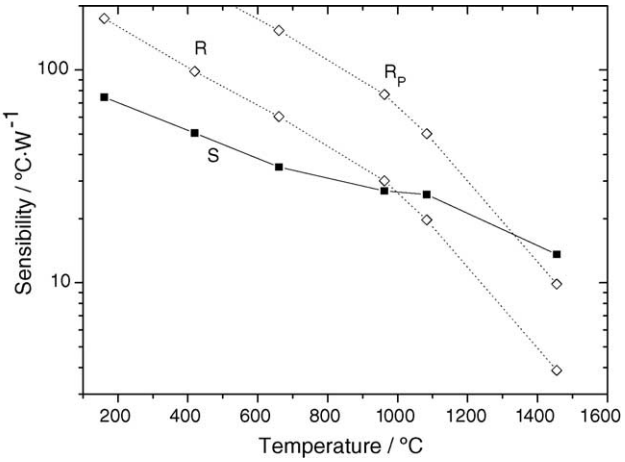

Fig. 9. Comparison between the sensitivity (S) and the thermal resistances R and R_P.

The reason is that the thermal resistance with the furnace is approximately proportional to the inverse of the exposed surface area, A. As the heat capacity is proportional to the mass, m, it follows that τ_{LAG} is nearly proportional to m/A. This ratio is 0.21 and 0.18 g/cm^2 for the pan and the pan and holder, respectively. Furthermore, according to Eq. (4), the thermal-lag differences between holder, pan and arm are smoothed out. This independence of τ_{LAG} from the model used in the calculation is an additional indication of the validity of the analysis.

4.2. Thermal models and temperature

In contrast with τ_{LAG}, sensitivity is much more dependent on the thermal model. Consequently, the question now arises about which model describes the signal better: Model B or Model C in Fig. 2. In this section we will show that, due to the temperature dependence of most thermal resistances, the calorimeter behavior switches progressively from one model to the other as temperature increases.

For this purpose, all the resistances in Fig. 2a have been calculated. R and R_P can be obtained from the experimental values of τ_{LAG} simply by dividing them by the heat capacity of the holder and pan ($R = \tau_{LAG}/C_{REF}$) or the pan only ($R_P = \tau_{LAG}/C_P$). R_H is then obtained from R and R_P. The 'leak resistances', R_{HP} and R_{AH}, are calculated from the geometry of the thermal contacts and thermal conductivities of the materials involved. The pan is in contact with the sample–holder by means of a thin platinum disc. This thermal resistance can be calculated with accuracy thanks to its cylindrical geometry:

$$R_{Pt} = \frac{1}{2\pi\kappa_{Pt}h_{Pt}} \ln\frac{D_{Pt}}{D_{pan}} \quad (13)$$

The result is plotted in Fig. 8. The deviation of R_{HP} from R_{Pt} is not clear because the contact resistance between the platinum disc and the alumina sample–holder have an effect whose sign is difficult to predict. Finally, the resistance between holder and arm is due to an alumina connection with a length of 3 mm and section 5.8 mm^2. We consider that the resistance of this alumina rod, R_{Al}, is in fact, a lower bound to the real value of R_{AH} because of the additional resistance to heat flow due to the sample–holder itself (in Fig. 8 the curve labeled 'R_{AH}' is in fact the value of R_{Al}).

In Fig. 8 the approximate values of all the relevant thermal resistances are plotted. From their relative values a clear evolution of the thermal model as the temperature increases can be deduced. Model B holds when $R_{HP} \ll R_P$, whereas Model C can be used when $R_{AH} \gg R_H$. Although the transition temperature from one model to the other one cannot be established with accuracy, we can say that it occurs in the 900–1100 °C range.

4.3. Understanding the sensitivity values (S)

The interpretation of the evolution of S with temperature (Fig. 9) is now straightforward if we apply the theory outlined in Section 2 to the information in Fig. 8. At low temperatures, Model B holds with significant thermal losses to the arm because $R_{AH} < R$. So, $S < R$. This loss of sensitivity diminishes as the temperature increases and S approaches R (Fig. 9). At high temperatures, the Model C holds and S reaches the maximum value R_P. In the intermediate temperature range, the thermal conditions switch progressively from one model to the other. Consequently, in spite of thermal losses to the arm diminishing progressively, S does not tend asymptotically to R (Fig. 9), but its experimental values cross the R curve at around 1000 °C. At higher temperatures, the slope of S with temperature increases, approaching the evolution of the pan-to-furnace resistance (R_P). Although at 1455 °C the values of S and R_P do not match exactly, this discrepancy can be tolerated in view of the simplicity of the model and the difficulties in calculating the exact values of the thermal resistances.

5. Discussion and conclusions

Despite the complicated geometry of our DTA apparatus (see Fig. 1), we have been able to modelize it with a RC model (Model A of Fig. 2) and calculate the main 'thermal masses' (*C*'s in Fig. 2) and 'thermal resistances' connecting them. This calculation has been done analytically and explains satisfactorily the absolute values and the evolution with temperature of τ_{LAG} and sensitivity, *without the need of any fitting parameter*. This result has been obtained thanks to a number of geometrical simplifications that are indicated throughout the text. Additionally, thermal contact resistances have been neglected and the furnace temperature has been taken as homogeneous. In a further step, one could try to do the analysis without someone of these simplifications, however, this will necessarily modify the method substantially. If thermal contact conductances are considered, it will require the introduction of several fitting parameters. If a non-homogeneous temperature of the furnace is considered, then a finite element analysis will be necessary and the merit of our analytical approach will be lost. We do not know the effect of these two simplifications on the numerical values, however we are convinced that nothing essential will be modified, since there is good agreement between measurements and predictions.

The main virtue of our analytical, although semi quantitative, approach is that it allows understanding the main paths through which heat is exchanged between the furnace and the sample. In particular, it has been shown that, due to the progressive increase of the radiative conductances with temperature, the 'complete' Model A can be simplified and reduces to Model B and Model C at low and high temperature, respectively (Fig. 8).

In our opinion, this work can help to improve the performance of similar DTA equipment. Within the simplest ideal Model B without thermal contact to the arm, sensitivity and peak width (given, approximately, by τ_{LAG}) are both proportional to *R*. So, apparently the improvement of one parameter is done at the expense of the other one. However, we have shown the crucial importance of the 'leak resistances' (R_{AH} and R_{HP}). As temperature increases, the sample becomes progressively isolated from the arm and the sample–holder and, consequently, sensitivity increases without compromising the peak width or resolution (related to τ_{LAG}). The value of the sensitivity at 1500 °C is the maximum value that one would expect from the geometrical construction of our DTA thanks to the fact that the sample is isolated from the holder. On the opposite temperature range, in an ideal situation without leak resistances, the sensitivity at 200 °C would be around eight times higher than the experimental value (compare R_P and *S* in Fig. 9). This example clearly shows that, by following the kind of analysis in this paper, alternative designs of furnace and sample–holder should allow significant improvements in the DTA signal quality.

The general conclusions that follow can be extended to other DTA equipment where heat exchange between sample and furnace is done by radiation and conduction through the gas:

(1) Thermal radiation is the main transport mechanism. Near room temperature, conduction through the gas can have an influence but can only dominate over radiation for high-conductivity gases like He.
(2) T^{-3} dependence of the resistance due to radiation explains the pronounced diminution of the apparatus sensitivity and τ_{LAG} as temperature increases. As a consequence, at higher temperatures peaks become narrower at the expense of sensitivity. At low temperatures, the main limitation is the low resolution (high values of τ_{LAG}).
(3) In contrast with most differential scanning calorimeters (DSC), where heat conduction dominates over radiation, the pronounced variation of the thermal resistances with temperature makes it necessary to use several RC models depending on the temperature range.

Acknowledgements

This work was supported by the Spanish Programa Nacional de Materiales under contract no. MAT-2002-04236-C04-02.

Appendix A. Derivation of τ_{LAG} of Model B and Model C

Consider, first, the Model B of Fig. 2b. Since the arm is very long (Fig. 1), its temperature will not be homogeneous. So, by T_{ARM} we mean its temperature on the side in contact with the holder. When the furnace is heated at a constant rate, β:

$$T_F = \beta t + T_F(0) \tag{A.1}$$

any point in contact with it will be progressively heated and, after a transient period, it will acquire the same heating rate. In the case of the sample and holder temperature, T_S, we can write:

$$T_S = T_F - \tau_{LAG}\beta \tag{A.2}$$

An elementary thermal balance relates the heating rate with the heat power that is absorbed by the sample and holder:

$$\phi_{REF} = C_{REF}\beta \tag{A.3}$$

whereas ϕ_{REF} can be calculated, too, by considering the heat 'conduction' through the thermal resistances:

$$\phi_{REF} = \frac{T_F - T_S}{R} + \frac{T_{ARM} - T_S}{R_{AH}} \tag{A.4}$$

Substitution of Eqs. (A.1) and (A.2) in Eq. (A.4) and elimination of ϕ_{REF} by subtracting Eq. (A.3) from Eq. (A.4) leads

to the desired result:

$$\tau_{\mathrm{LAG}}(\text{Model B}) = RC_{\mathrm{REF}} + \frac{T_{\mathrm{S}} - T_{\mathrm{ARM}}}{\beta}\frac{R}{R_{\mathrm{AH}}} \tag{A.5}$$

For the calculation of τ_{LAG} for Model C (Fig. 2c) we follow a similar procedure. The sample and holder temperatures (T_{S} and T_{H}) will lag behind the furnace temperature according to:

$$T_{\mathrm{S}} = T_{\mathrm{F}} - \tau_{\mathrm{LAG}}\beta \quad \text{and} \quad T_{\mathrm{H}} = T_{\mathrm{F}} - \tau_{\mathrm{H}}\beta \tag{A.6}$$

From the thermal balance, the heating rate can be related to the temperatures for both sample and holder:

$$C_{\mathrm{P}}\beta = \frac{T_{\mathrm{F}} - T_{\mathrm{S}}}{R_{\mathrm{P}}} + \frac{T_{\mathrm{H}} - T_{\mathrm{S}}}{R_{\mathrm{HP}}} \quad \text{and}$$

$$C_{\mathrm{H}}\beta = \frac{T_{\mathrm{F}} - T_{\mathrm{H}}}{R_{\mathrm{H}}} + \frac{T_{\mathrm{S}} - T_{\mathrm{H}}}{R_{\mathrm{HP}}} \tag{A.7}$$

Introduction of Eqs. (A.6) and (A.1) into (A.7) leads to:

$$C_{\mathrm{P}} = \frac{\tau_{\mathrm{LAG}}}{R_{\mathrm{P}}//R_{\mathrm{HP}}} - \frac{\tau_{\mathrm{H}}}{R_{\mathrm{HP}}} \quad \text{and}$$

$$C_{\mathrm{H}} = \frac{\tau_{\mathrm{H}}}{R_{\mathrm{H}}//R_{\mathrm{HP}}} - \frac{\tau_{\mathrm{LAG}}}{R_{\mathrm{HP}}} \tag{A.8}$$

from which the value of τ_{LAG} can be obtained:

$$\tau_{\mathrm{LAG}}(\text{Model C}) = \frac{R_{\mathrm{H}} + R_{\mathrm{HP}}}{R_{\mathrm{P}} + R_{\mathrm{HP}} + R_{\mathrm{H}}}R_{\mathrm{P}}C_{\mathrm{P}} + \frac{R_{\mathrm{P}}}{R_{\mathrm{P}} + R_{\mathrm{HP}} + R_{\mathrm{H}}}R_{\mathrm{H}}C_{\mathrm{H}} \tag{A.9}$$

References

[1] M.J. Richardson, Thermochim. Acta 300 (1997) 15.
[2] M.E. Patt, B.E. White, B. Stein, E.J. Cotts, Thermochim. Acta 197 (1992) 413.
[3] G.W.H. Höhne, W. Hemminger, H.-J. Flammersheim, Differential Scanning Calorimetry, Springer, Berlin, 1996.
[4] Y. Saito, K. Saito, T. Atake, Thermochim. Acta 107 (1986) 277.
[5] S.C. Mraw, Rev. Sci. Instrum. 53 (1982) 228.
[6] Y. Saito, K. Saito, T. Atake, Thermochim. Acta 99 (1986) 299.
[7] J.S. Crighton, F.W. Wilburn, Thermochim. Acta 203 (1992) 1.
[8] M.J. Richardson, N.G. Savill, Thermochim. Acta 12 (1975) 213.
[9] F.U. Buehler, J.C. Seferis, Thermochim. Acta 334 (1999) 49.
[10] J.P.A. Neeft, F. Hoornaert, M. Makkee, J.A. Moulijn, Thermochim. Acta 287 (1996) 261.
[11] R. Melling, F.W. Wilburn, R.M. McIntosh, Anal. Chem. 41 (1969) 1275.
[12] J. Font, J. Muntasell, J. Navarro, E. Cesari, Thermochim. Acta 88 (1985) 425.
[13] T. Ozawa, Thermochim. Acta 355 (2000) 35.
[14] S.L. Boersma, J. Am. Ceram. Soc. 38 (1955) 281.
[15] F.W. Wilburn, D. Dollimore, J.S. Crighton, Thermochim. Acta 181 (1991) 191.
[16] F.U. Buehler, J.C. Seferis, Thermochim. Acta 334 (1999) 49.
[17] I. Hatta, R. Kato, A. Maesono, Jpn. J. Appl. Phys. 26 (1987) 475.
[18] T. Fujino, T. Kurosawa, Y. Miyata, K. Naito, J. Phys. E: Sci. Instrum. 4 (1971) 51.
[19] W.M. Rohsenow, J.P. Hartnett, Y.I. Cho (Eds.), Handbook of Heat Transfer, 3rd ed., McGraw-Hill, New York, 1998.
[20] W.D. Kingery, H.K. Bowen, D.R. Uhlmann, Introduction to Ceramics, 2nd ed., Wiley, New York, 1976.
[21] T.C.K. Yang, D.S. Viswanath, J. Am. Ceram. Soc. 80 (1997) 157.
[22] C. Rath, J. Farjas, P. Roura, Thermochim. Acta 412 (2004) 113.